Structural and electronic properties of 13-atom 4*d* transition-metal clusters

Yan Sun,[1] René Fournier,[2,*] and Min Zhang[1]
[1]*Department of Physics, York University, Toronto, Ontario, Canada M3J 1P3*
[2]*Department of Chemistry, York University, Toronto, Ontario, Canada M3J 1P3*
(Received 18 July 2008; revised manuscript received 20 January 2009; published 10 April 2009)

We performed global optimization and property calculations by density-functional theory for the series of 4*d* transition-metal clusters M_{13}, $M=\mathrm{Y}-\mathrm{Pd}$. Calculated Gibbs free energies suggest the coexistence of isomers, or spin states, other than the global minimum in all cases except maybe Zr_{13} and Pd_{13}. The calculated infrared spectra of these isomers are typically very different. Calculated ionization energies and magnetic moments agree well with available experimental results but do not allow to assign the geometric structure. Analysis of relative isomer energies and their electronic density of states suggests that these clusters tend to follow a maximum hardness principle: the lowest energy states and geometric structures are often the ones with lowest density of states near the Fermi level and lowest spin magnetic moment. In going from left to right in the 4*d* series, the geometric structures evolve from icosahedral (Y, Zr), to distorted compact structures (Nb, Mo), to fcc or simple-cubic crystal fragments (Tc, Ru, Rh), and icosahedron again (Pd). We rationalize this trend on the basis of the increasingly localized nature of molecular orbitals in going from left to right and the importance of *d*-type orbital bonding in the middle of the series.

DOI: 10.1103/PhysRevA.79.043202 PACS number(s): 36.40.Mr, 31.10.+z, 61.46.Bc

I. INTRODUCTION

Clusters of 4*d* transition-metal (TM) elements have attracted a lot of attention because of their unusual electronic and magnetic properties compared to their bulk counterparts [1]. These properties depend on the geometric and electronic structures of the lowest energy isomers, which makes the search of the global minimum (GM) very important. The possibility of coexisting low-energy isomers with different spin states adds a lot of difficulty to the study of the geometric [2] and electronic properties of 4*d* TM clusters [3,4]. Recent first-principles calculations showed that the ground-state structures for most 13-atom TM clusters do not favor high-symmetry compact structures. Instead, there are less symmetric structures such as cubic [5] and buckled biplanar (BBP) [6] structures lying significantly lower in energy than the icosahedral (ico) isomers found earlier. Wang and Johnson [7] found a low-symmetry open structure to be most stable for Pd_{13}. Theory predicts the GM to be a cubic structure for both Ru_{13} [8] and Rh_{13} [5]. Rogan *et al.* [9] found another biplanar structure lowest in energy for Rh_{13}.

Recently, we studied periodic trends in GM structures of 13-atom clusters for 26 elements (including the 4*d* transition metals) obtained by global optimization with the energy evaluated by density-functional theory [10]. We found much diversity among these structures and showed how this is related to different atomic properties and types of bonding. Here we report a more detailed study of structures, energies, and properties of the GM and also the low-energy isomers for the series of 13-atom 4*d* TM clusters, calculated for different spin states and with different exchange-correlation functionals. By considering geometries and spin states other than those of the GM, we are able to study the interplay between geometric and electronic structures. We will also discuss the possible coexistence of isomers in experiments and the effect this may have on measured ionization energies, magnetic moments, and infrared spectra. We will now briefly review some experimental and theoretical results.

The measured vertical ionization potentials (VIPs) are 4.10 ± 0.05 eV for Y_{13} [11] and 4.85 ± 0.05 eV for Nb_{13} [4]. The measured vertical electron affinity (VEA) of Nb_{13} is 1.70 ± 0.05 eV [12]. Stern-Gerlach experiments allow estimates of spin magnetic moments ($2S$) and indicate that some TM clusters are magnetic although their bulk counterpart is not. The measured magnetic moments are $8.8\pm0.1\mu_B$ for Y_{13} [13], somewhere between $4.6\mu_B$ and $7.9\mu_B$ for Rh_{13} [14], less than $3.8\mu_B$ for Ru_{13} [14], and less than $5.2\mu_B$ for Pd_{13} [14]. Yuan *et al.* [15] predicted a magnetic moment of $19\mu_B$ for Y_{13} by density-functional calculation. Similarly, Li *et al.* [8] found $4\mu_B$ for Ru_{13}. Calculations by Wang and Johnson [7] predicted magnetic moments of $9\mu_B$ for Rh_{13} and $6\mu_B$ for Pd_{13}. As we will show later (see Tables III and IV), our calculations suggest that there are between two and four different spin states within 3 kcal/mol of the ground state in every case.

II. COMPUTATIONAL METHODS

Putative GM from Y_{13} to Pd_{13} were obtained by global optimization with no *a priori* assumption about structure. The calculations combined the taboo search in descriptor space (TSDS) global optimization method [16] with an energy evaluated with the GAUSSIAN03 software [17] using the Los Alamos National Laboratory double-zeta (LANL2DZ) effective core potential and basis sets and the local spin-density (LSD) approximation, followed by local optimizations with either the 3-parameter Becke-Lee-Yang-Parr (B3LYP) or Perdew-Burke-Ernzerhof (PBE) exchange-correlation (xc) functional [18]. The TSDS-LSD searches consisted of 700 steps, with one new structure and one energy evaluation at each step. The strategy in TSDS is to

*renef@yorku.ca

TABLE I. Dissociation energy (D_0 in eV) and equilibrium bond length R_e (in Å) of metal dimers calculated by LSD, B3LYP, and PBE functionals. The spin magnetic moment ($2S$) for the ground state is 4 for Y [20], 0 for Zr (but Wang *et al.* [23] found $2S=2$), 2 for Nb, 0 for Mo, 6 for Ru, 4 for Rh, and 2 for Pd.

Experimental		LSD		B3LYP		PBE	
D_0	R_e	D_0	R_e	D_0	R_e	D_0	R_e
Y_2:							
1.62 ± 0.22 [21]							
2.16 [15]	2.956 [15]	2.15	2.92	0.87	2.95	1.67	2.95
Zr_2:							
3.052 ± 0.001 [22]							
3.004 [23]	2.032 [23]	4.60	2.32	2.57	2.33	3.77	2.34
Nb_2:							
4.80 ± 0.05 [24]							
5.22 ± 0.05 [25]							
5.22 [26]							
5.48 [27]	2.078 [24]	5.92	2.13	3.51	2.13	4.47	2.14
Mo_2:							
4.38 ± 0.10 [28]	1.94 [28]						
4.29 ± 0.02 [29]	1.938 [29]	4.50	1.98	1.68	1.94	3.07	1.94
Ru_2:							
3.19 [30]	2.25 [30]	4.55	2.26	1.88	2.28	3.22	2.29
Rh_2:							
2.92 ± 0.22[31]	2.28 [31]	4.34	2.23	1.40	2.32	2.98	2.26
Pd_2:							
1.03 ± 0.16 [32]							
1.41 [33]	2.65 [32]	1.92	2.45	1.02	2.53	1.52	2.51

generate nuclear configurations that are very dissimilar in the early stages (exploration) and to gradually switch selection criteria so that, in later stages, the nuclear configurations that get generated (and selected) resemble, but are not identical to, the lowest energy structures found up to that point (exploitation) [19]. After those 700 iterations, the 15 lowest energy distinct structures were passed to GAUSSIAN03 for local optimization (B3LYP or PBE). We did vibrational analysis by PBE theory for all the low-energy isomers reported in Fig. 1 and found that all of them have 33 real fundamental frequencies, i.e., they are true minima. Besides, we also did local optimizations using PBE theory for low-energy structures previously reported in the literature. Different spin multiplicities were considered in each case. More details about TSDS and the procedures we used to find the lowest energy isomers can be found in the supplementary material [19]. Test calculations for TM diatomic were performed by three different functionals: LSD, B3LYP, and PBE functionals. Results such as equilibrium distance R_e and dissociation energy D_0 are compared to the available experimental and theoretical data in Table I. On the whole, PBE functional gives the best agreement with experiments so we use the PBE optimized structures and results in the following analysis of geometric and electronic properties for all the structures (GM and isomers).

TABLE II. Calculated total electronic energy relative to GM (RE) and spin magnetic moment for all isomers in Fig. 1. For GM, the VIP, VEA, and HOMO-LUMO gap values are also given (in eV).

	B3LYP	PBE
Y_{13a}	0; 19; 4.10; 1.43; 0.92	0; 19; 4.20; 1.56; 0.16
Y_{13b}	0.35; 1	0.31; 1
Zr_{13}	0; 6; 4.43; 1.54; 0.94	0; 6; 4.76; 1.62; 0.18
Nb_{13a}	0; 1; 4.56; 1.46; 1.03	0; 1; 4.69; 1.51; 0.24
Nb_{13b}	0.27; 1	0.09; 1
Nb_{13c}	0.15; 3	0.20; 3
Mo_{13a}	0; 2; 4.61; 1.45; 1.07	0; 0; 4.72; 1.58; 0.21
Mo_{13b}	0.29; 4	0.07; 0
Mo_{13c}	0.34; 4	0.20; 4
Tc_{13}	0; 1; 6.02; 1.10; 1.08	0; 1; 5.21; 1.99; 0.16
Ru_{13}	0; 6; 5.63; 2.30; 1.22	0; 2; 5.62; 2.28; 0.11
Rh_{13a}	1.18; 7	0; 1; 6.94; 2.51; 0.19
Rh_{13b}	0; 1; 5.73; 2.28; 0.99	0.68; 15
Pd_{13a}	0.20; 8	0; 8; 6.44; 2.78; 0.12
Pd_{13b}	0; 6; 6.45; 2.55; 1.33	0.01; 6
Pd_{13c}	0.08; 6	0.31; 6

III. RESULTS AND DISCUSSION

A. Structures

All isomers found within 0.5 eV of the GM are shown in Fig. 1 and their spin states and relative energies (REs) calculated by two functionals are in Table II. We only show the ground state for each structure but there are actually many different spin states, each with a slightly different geometry and energy (differences smaller than 0.3 eV). For each GM, the VIP, VEA, and highest occupied molecular orbital–lowest unoccupied molecular orbital (HOMO-LUMO) gap are also listed in Table II. Figure 2 shows the RE to GM calculated by PBE functional. Typical structures in Fig. 1 can be described as high-symmetry structures such as ico, dis-

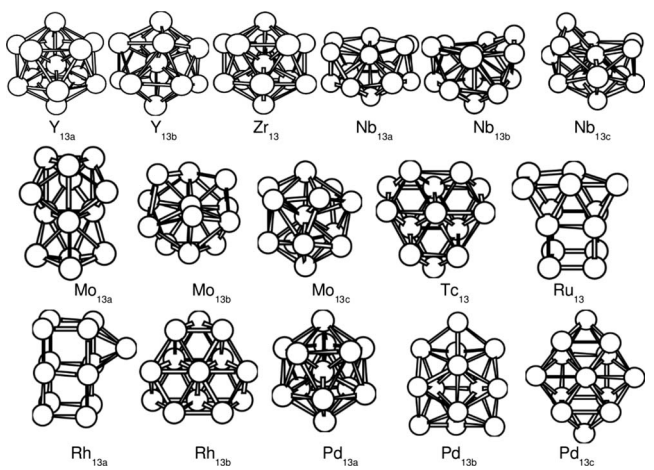

FIG. 1. The geometric structures for the GM ($13a$) and isomers within 0.5 eV of the GM for Y_{13} to Pd_{13}.

TABLE III. Calculated relative electronic energy (RE), total energy (E+ZPE), zero-point correction (ZPE), TS (T=298 K and S is the entropy), relative enthalpy (RH), and relative free energy (RG) calculated with G03 [48] for low-energy isomers of Y, Zr, Nb, and Mo. All energies are in kcal/mol except (E+ZPE) in hartree.

	2S	RE	E+ZPE	ZPE	TS	RH	RG
Y_{13a}	19	0	−493.168092	5.34	59.47	0	2.34
	17	0.23	−493.167781	5.02	60.94	0.20	0
	13	1.38	−493.166173	4.60	63.02	1.20	0
	11	5.07	−493.160150	4.45	63.29	4.98	3.51
Y_{13b}	7	7.38	−493.156354	4.83	61.76	7.37	7.42
	1	7.15	−493.156823	4.88	60.68	7.07	8.20
Zr_{13}	6	0	−605.489511	6.44	56.81	0	0
	2	4.38	−605.482651	6.16	57.45	4.30	3.64
	0	5.30	−605.480937	6.60	54.53	5.38	7.65
Nb_{13a}	1	0	−732.368799	8.37	50.86	0	0
	3	5.77	−732.359619	8.26	51.85	5.76	4.92
Nb_{13b}	1	2.07	−732.365588	7.85	52.66	2.01	0.21
Nb_{13c}	3	4.61	−732.361602	8.20	52.22	4.52	3.15
Mo_{13a}	0	0	−878.165057	8.85	49.71	0	0.39
	2	0.46	−878.164485	8.87	50.46	0.36	0
	4	5.07	−878.157101	8.75	50.57	4.99	4.52
Mo_{13b}	0	1.61	−878.162605	8.41	51.14	1.54	0.50
	4	5.30	−878.156980	8.24	52.20	5.07	2.97
Mo_{13c}	4	4.61	−878.157970	7.88	54.28	4.45	0.27

TABLE IV. Calculated relative electronic energy (RE), total energy (E+ZPE), zero-point correction (ZPE), TS (T=298 K and S is the entropy), relative enthalpy (RH), and relative free energy (RG) calculated with G03 [48] for low-energy isomers of Tc, Ru, Rh, and Pd. All energies are in kcal/mol except (E+ZPE) in hartree.

	2S	RE	E+ZPE	ZPE	TS	RH	RG
Tc_{13}	1	0	−1041.306 311	9.40	48.40	0	0.01
	3	1.61	−1041.303 926	9.03	49.91	1.50	0
	5	3.00	−1041.301 636	9.20	49.40	2.93	1.94
Ru_{13}	2	0	−1220.906 577	9.38	48.91	0	0.36
	4	0.46	−1220.905 895	9.22	49.70	0.43	0
	6	2.08	−1220.903 364	8.98	50.97	2.02	0.32
Rh_{13a}	1	0	−1423.979 455	8.40	50.72	0	0
	3	3.92	−1423.973 657	8.54	50.72	3.64	3.74
	5	6.00	−1423.970 037	8.54	50.87	5.91	5.76
	7	3.46	−1423.974 116	8.31	51.67	3.35	2.40
	9	1.85	−1423.976 708	8.42	51.55	1.72	0.89
Rh_{13b}	15	15.30	−1423.955 746	6.73	56.23	14.88	9.36
	17	15.45	−1423.955 632	6.49	57.69	14.95	7.98
Pd_{13a}	8	0	−1647.898 500	5.14	60.63	0	0
	4	7.84	−1647.886 121	5.01	61.04	7.77	7.36
	2	8.30	−1647.885 060	5.30	59.31	8.43	9.76
Pd_{13b}	6	0.23	−1647.898 005	5.83	58.09	0.31	2.86
	4	3.00	−1647.893 668	5.76	58.33	3.03	5.33
	2	3.69	−1647.892 105	5.85	57.67	4.01	6.97
	8	8.07	−1647.885 440	5.75	58.92	8.20	9.91
Pd_{13c}	6	7.15	−1647.886 930	5.65	59.27	7.26	8.62
	2	8.99	−1647.883 848	5.62	59.19	9.19	10.64

torted ico structures, hcp or fcc crystal fragments, cubic structures, and biplanar structures such as BBP.

The Y_{13} GMs found by B3LYP and PBE functionals both have the ico structure with a magnetic moment equal to $19\mu_B$ which agrees with the results of Yuan *et al.* [15]. There are many possible spin states, but it is impossible at present for us to carry a full global optimization on each of the spin state energy surface of Y_{13}. For ico Y_{13}, the GM shown in Fig. 1, the lowest energy spin state is $2S=19$. We also found five local minima within 0.32 eV of this GM: three of them ($2S=17,13,11$) have almost ideal ico structures, such as Y_{13a} in Fig. 1, and the other two ($2S=7,1$) have the distorted ico structure Y_{13b} shown in Fig. 1. It is clear that other spin states of ico Y_{13} would give slightly different geometries, and energies roughly +0.3 eV above the GM. As the 2S values decrease from 19 to 1, structures deviate further from the ideal ico and the relative energies to the GM increase from 0 to 0.32 eV which shows that Y_{13} prefers high-symmetry structures. This can be rationalized from the $4d5s^2$ electronic configuration and small effective nuclear charge of the Y atom: the delocalized s electrons dominate the electronic structure leading to the high-symmetry ico structures. We have at least three low-energy ico isomers that match the experimental VIP (4.10 ± 0.05 eV [11]) very well: $Y_{13}(2S=19)$ has a VIP of 4.11 eV by B3LYP functional and 4.20 eV by PBE functional, $Y_{13}(2S=13)$ has 4.00 eV by B3LYP functional and 4.17 eV by PBE functional, and $Y_{13}(2S=1)$ has 4.08 eV by B3LYP functional and 4.56 eV by PBE functional. We cannot distinguish between these isomers by comparing our calculations to photoelectron spectroscopy.

The GMs found for Zr_{13} by B3LYP and PBE functionals have the same slightly distorted ico structure as Y_{13} with a magnetic moment of $6\mu_B$. This agrees with the calculation of Chang and Chou [6]. The ideal ico relaxed to the structure shown in Fig. 1 with bond lengths that vary in the range of 2.87–3.28 Å including two short bonds of 2.87 Å, 38 bonds in the range 2.91–3.15 Å, and two outer-shell bonds of 3.27 Å. There are two slightly distorted ico isomers

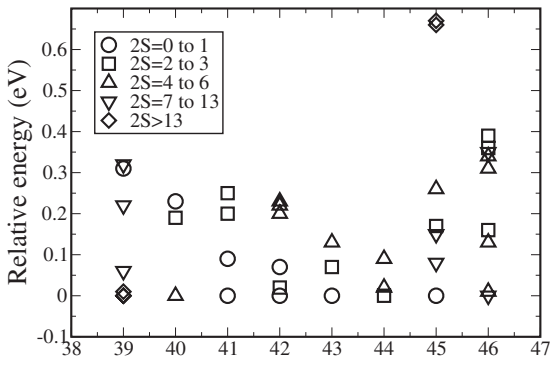

FIG. 2. Relative energies of A_{13} low-energy isomers in eV, from Y to Pd (atomic numbers 39–46).

$(2S=0,2)$ within 0.23 eV of the GM. The lowest energy non-ico isomer found by TSDS is roughly 1.14 eV above the GM so we can rule it out.

The GM of Nb_{13} is a severely distorted ico (Nb_{13a} in Fig. 1) with a spin magnetic moment of $1\mu_B$. Distorted ico structures with different spin states have been proposed as possible GMs by different groups: Kumar and Kawazoe $(2S=3\mu_B)$ [34], Chang and Chou $(2S=3\mu_B)$ [6], Fa *et al.* [35], and Deng *et al.* $(2S=7\mu_B)$ [36]. These results also differ in structural details such as the bond lengths. After several local optimizations we found four isomers within 0.25 eV of each other. Two have the Nb_{13a} structure with $2S=1$ (RE=0 eV, the GM) and $2S=3$ (RE=0.25 eV), one is the Nb_{13b} structure with $2S=1$ (RE=0.09 eV), and the fourth one is a less distorted ico Nb_{13c} that originates from the ideal ico with $2S=3$ (RE=0.20 eV). Higher spin states $2S=5,7$ for structures (a)–(c) in Fig. 1 produced isomers that are 0.64 eV or higher relative to the GM. Apparently, low-energy isomers of Nb_{13} tend to have relatively flat structures and low spin. We got the VIP value for the GM $Nb_{13a}(2S=1)$ as 4.56 eV (B3LYP) and 4.69 eV (PBE), and VEA as 1.46 eV (B3LYP) and 1.51 eV (PBE). Both agree very well with the experimental values, 4.84 ± 0.05 eV [4] (VIP) and 1.70 ± 0.05 eV [12] (VEA). We do not show the calculated VIP and VEA values for all the isomers since we have the same situation as for Y_{13} in that all isomers have similar VIP and VEA values making them hard to distinguish experimentally.

Chang and Chou [6] found a very distorted ico with $2S=8$ to be a stable isomer for Mo_{13}. Zhang *et al.* [37] also found that a severely distorted ico $2S=2$ was more stable than the high-symmetry ico. Deng *et al.* [36] got an fcc lattice fragment (O_h) with $2S=2$ as the most stable among many high-symmetry isomers. We found six low-energy isomers. Three of them have the Mo_{13a} structure with $2S=0$ (RE=0.00 eV), $2S=2$ (RE=0.02 eV), and $2S=4$ (RE=0.22 eV), two have the Mo_{13b} structure with $2S=0$ (RE=0.07 eV) and $2S=4$ (RE=0.23 eV), and the sixth one has a distorted ico structure (Mo_{13c} in Fig. 1) with $2S=4$ (RE=0.20 eV). Other structures we considered have a much higher energy: ideal ico (RE=0.94 eV), O_h fcc fragment (RE=1.36 eV), and D_{3h} hcp fragment (RE=1.70 eV).

The GM we find for Tc_{13} is a two-layer fragment of the fcc (or hcp) lattice with almost no distortion. The energy is lowest for spin state $2S=1$, then $2S=3$ (RE=0.07 eV) and $2S=5$ (RE=0.13 eV). Locally optimized ico structures are significantly distorted and lie at least 1.65 eV higher than the GM, showing that Tc_{13} has a strong tendency to form more extended structures.

For Ru_{13} we got the same cubic structure GM as Li *et al.* [8] with the same spin magnetic moment $2\mu_B$, which agrees well with the experimental results $(2S\leq3.77\mu_B)$. There were two other isomers having the same structure but different $2S$ values close to the GM, $2S=4$ with RE=0.02 eV and $2S=6$ with RE=0.09 eV. The lowest energy structure found by TSDS is a distorted two-layer fcc fragment similar to the GM of Tc_{13} and lies 2.00 eV higher in energy than the cubic GM.

The Rh_{13} GM found by B3LYP functional is a biplanar structure (Rh_{13b} in Fig. 1) similar to the GM of Tc_{13}, with a spin magnetic moment equal to $17\mu_B$. Futschek *et al.* [38] proposed this structure as the possible GM for Rh_{13} and Pd_{13} based on dynamic simulated annealing density-functional theory (generalized gradient approximation) calculations. The ground-state magnetic moment they found for that geometry was $13\mu_B$ for Rh_{13} and $6\mu_B$ for Pd_{13}. Rogan *et al.* [9] found the same Rh_{13} structure with $2S$ equal to $13\mu_B$ and another isomer $(2S=15)$ 0.19 eV higher. The GM we found by PBE functional is very different; it has a cubic structure [5] (Rh_{13a} in Fig. 1) with $2S=1$. According to PBE functional, there are four low-energy isomers within 0.26 eV having basically the same cubic structure with $2S=3$ (RE=0.17 eV), $2S=5$ (RE=0.26 eV), $2S=7$ (RE=0.15 eV), and $2S=9$ (RE=0.08 eV). The Rh_{13a} isomer is 1.18 eV higher than Rh_{13b} according to B3LYP functional, whereas Rh_{13b} is 0.68 eV higher than Rh_{13a} by PBE functional. This is the only case in our calculations where the two functionals give completely different GM: one with $2S=17\mu_B$ and the other with $2S=1\mu_B$. Note that the structures of Pd_{13a} (the PBE GM) and Pd_{13b} (the B3LYP GM) differ a lot, but their relative energies calculated by B3LYP (0.20 and 0.00 eV, respectively) and PBE (0.00 and 0.01 eV, respectively) functionals are very close and their spin states are similar.

We found nine low-energy isomers of Pd_{13} within 0.39 eV of the GM by PBE. The GM is an ico structure (Pd_{13a} in Fig. 1) with $2S=8$. There are two other ico isomers with $2S=4$ (RE=0.34 eV) and $2S=2$ (RE=0.36 eV). Pd_{13b} in Fig. 1 was found by TSDS. It is similar to the GM proposed by Wang and Johnson [7]. There are four isomers based on this structure: $2S=6$ (RE=0.01 eV), $2S=4$ (RE=0.13 eV), $2S=2$ (RE=0.16 eV), and $2S=8$ (RE=0.35 eV). The other two isomers have the Pd_{13c} structure with $2S=6$ (RE=0.31 eV) and $2S=2$ (RE=0.39 eV). According to B3LYP functional, Pd_{13b} with $2S=6$ is lowest in energy, with Pd_{13a} 0.20 eV higher. This is another example where different functionals lead to different GMs. It also shows that a global search performed for an arbitrary spin state (here $2S=0$) can easily miss the GM if that GM has a very different ground-state spin magnetic moment.

B. Comments on the performance of TSDS

The TSDS global optimization using the LSD approximation for xc and arbitrarily chosen spin states failed to find the lowest PBE energy structure (putative GM) in five out of eight cases: Nb, Mo, Ru, Rh, and Pd. There could be different reasons for that. The relative energies of Rh_{13} isomers and spin states are extremely sensitive to xc approximation: in this case, using LSD in the global search instead of PBE functional was bad. The TSDS-LSD search was partly successful for Nb_{13}, Mo_{13}, and Pd_{13} as it produced structures that are only 0.09, 0.07, and 0.01 eV higher than the GM, respectively. Longer TSDS searches with PBE functional for all relevant spin states would likely have found the $13a$ structures in those three cases. For Ru_{13}, the best structure TSDS-LSD generated is 2 eV higher than the GM and that seems to indicate a real problem with TSDS itself. After the fact, it appears the problem was in the choice of descriptors.

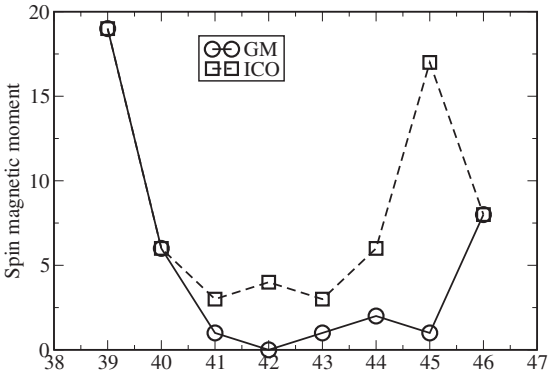

FIG. 3. Spin magnetic moment for GM and ico isomers from Y to Pd (atomic number 39–46).

In Ru_{13} (and Rh_{13}), *d–d* bonding is important and favors the formation of 90° bond angles, but this aspect of structure was not included among the descriptors used during the TSDS optimization. We believe that including the number of 90° angles among the descriptors (see the equation for R in Sec. III D) would have improved the TSDS search for Ru and Rh. This is an example of a more general problem with TSDS: the choice of descriptors can potentially bias the search. We think we can fix this problem in the future by having very many descriptors and letting the algorithm automatically select, in the course of each optimization run, a small subset of descriptors that is optimal in the sense of accurately interpolating DFT energies.

C. Magnetic moments

We plotted the spin magnetic moments of GM and ico structures in Fig. 3. The ico structures generally have larger spin magnetic moments than GM (note that Y_{13}, Zr_{13}, and Pd_{13} have ico as the GM), as had been suggested by Dunlap in a study of Fe_{13} isomers with high symmetry [39]. Furthermore, the non-ico low-energy isomers of Y_{13}, Zr_{13}, and Pd_{13} have a smaller ground-state magnetic moment than the ico GM (for example, $2S=6$ for Pd_{13b} and Pd_{13c} vs $2S=8$ for Pd_{13} GM). A rationale for this is the relation between magnetic moment and symmetry [39]. High-symmetry structures such as ico normally generate larger orbital degeneracy near the Fermi energy, resulting in larger spin magnetic moments. Note that in the ellipsoidal jellium model [40], which is relevant for *s*-type states, a jellium sphere exhibits degeneracies and undergoes deformation to a prolate or oblate geometry (depending on the number of electrons) when the effective number of delocalized electrons is in the range from 10 to 16 and that the effective number of delocalized *s* electrons in our clusters falls in that range (it is roughly 13). Among the eight clusters, three (Y_{13}, Zr_{13}, and Pd_{13}) are magnetic (Rh_{13} could be magnetic if we consider the coexisting isomers within 0.20 eV) although their bulk counterparts are not. There are discrepancies between the experimental result and our theoretical results in the case of Y_{13}, Rh_{13}, and Pd_{13}, which could be explained by the contribution from low-energy isomers with different spin multiplicity. For example, the measured spin magnetic moment for Y_{13} is $8.8\pm0.1\mu_B$ [13], which is smaller than for our GM ($2S=19\mu_B$). However, our calculations indicate at least five isomers with different spin states lying less than 0.32 eV above the GM, so the experimental results could be an average over several coexisting isomers with different spin states. Moreover, the order in isomers is different, and yields a smaller value of $2S$, if we use the Gibbs free energy instead of the energy (see Table III and Sec. III E).

The experimental $2S$ values for Rh_{13} are in the range of $4.55-7.93\mu_B$, and we get $2S=1$ for the GM. However we also found four isomers of Rh_{13} within 0.26 eV of the GM with $2S=3,5,7,9$ which could generate a range of $2S$ values like in the experiment. For Rh_{13}, the discrepancy between theoretical and experimental results has been discussed previously [5–7,9,38]. Wang and Johnson [7] found two isomers with $2S=1,3$ within 0.68 eV of the GM and suggested that the experimental $2S$ value could be an ensemble average. There are five isomers of Pd_{13} in Table III with $2S$ smaller than $6\mu_B$ within 0.4 eV of the GM, which could also satisfy the experimental result $2S<5.2\mu_B$ [14].

Aguilera-Granja *et al.* [41] did a theoretical study of the magnetism in Rh clusters and concluded that the coexistence of isomers would not have a big effect on observed magnetic moments. However, the geometric structures for their GM and low-energy isomers (essentially ico-based structures) were obtained with an empirical Gupta potential and are totally different from the structures predicted by DFT. Their GM has a very high PBE energy relative to our GM (Fig. 1) and is irrelevant according to PBE functional. More generally, the structures that we get (Fig. 1) are much more diverse than, and qualitatively different from, those normally found with empirical potentials [10].

Futscheck *et al.* [38] studied Rh_n and Pd_n ($n=2-13$) clusters by density-functional theory. They found several low-lying structural and magnetic isomers at various cluster sizes and discussed in detail the magnetic isomers. In particular, they pointed out that the temperature dependence of magnetic properties for these Rh_n and Pd_n clusters is far from simple. Our results qualitatively agree with this and show that magnetic isomers and nontrivial thermal averaging of magnetic properties are probably common to all second row TM clusters (see Tables III and IV).

According to Stoner's criterion for ferromagnetism [42], clusters tend to be magnetic when they have a large density of states (DOS) at the Fermi level. On the other hand, the maximum hardness principle [43–45] (MHP) states that, under certain conditions, larger values of [(VIP)−(VEA)] correlate with lower energy. In practical applications of the MHP, one often approximates [(VIP)−(VEA)] by the HOMO-LUMO gap. If we consider the two criteria, we would expect that metal clusters have a general tendency to adopt structures giving the lowest DOS value at the Fermi level, resulting in a tendency toward the lowest spin magnetic values ($2S$) in their ground electronic state. In order to test this hypothesis, we calculated, for the GM and all isomers, the number of states *near* the Fermi energy by using a Gaussian function centered at E_F with a width of 0.3 eV. We define the number of states $N(E_F)$ near E_F as

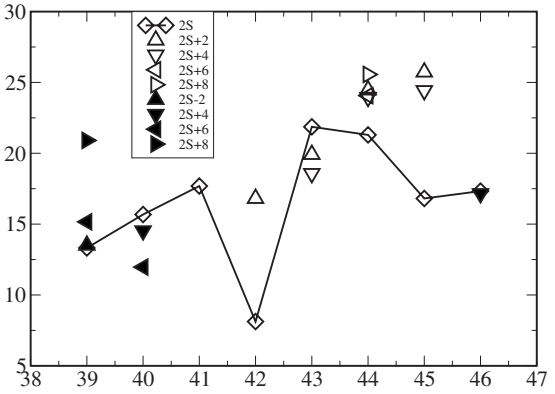

FIG. 4. Calculated values of $N(E_F;0.3)$ for GM and isomers with same structure but different $2S$ from Y to Pd (atomic numbers 39–46). The solid line connects the GM of each element.

$$N(E_F;0.3) = \sum_j g(e_j - E_F;0.3),$$

where $g(x-c;w)$ is a Gaussian function of width w [full width at half maximum (FWHM)], the e_j's are Kohn-Sham orbital energies, and all quantities are in eV. In order to find a reasonable width w for the Gaussian, we tried different values ranging from 0.1 to 0.5 eV and found that $w=0.3$ gives fairly stable results. For comparison, considering all the isomers in Fig. 1, the $N(E_F;0.3)$ values are smallest for Y_{13a}, Nb_{13a}, Mo_{13a}, Rh_{13a}, and Pd_{13a}, while the $N(E_F;0.5)$ values are smallest for Y_{13a}, Nb_{13b}, Mo_{13a}, Rh_{13b}, and Pd_{13a}. Figure 4 gives the calculated $N(E_F;0.3)$ from Y_{13} to Pd_{13} for the GMs and the available lower energy isomers based on the same structure with different $2S$ values. The GMs have a lower $N(E_F;0.3)$ value than any other spin state except for Zr_{13} and Tc_{13}, which generally agrees with the MHP. For Nb_{13}, Mo_{13}, Ru_{13}, and Rh_{13}, the GMs prefer the lowest spin state among all possible $2S$ values and these lowest spin states have the lowest $N(E_F;0.3)$ values compared to higher spin states, consistent with Stoner's criterion. We also compared the $N(E_F;0.3)$ values between isomers with truly different structures. In Fig. 5, the $N(E_F;0.3)$ values for low-energy isomers (within 0.5 eV to the GMs) based on

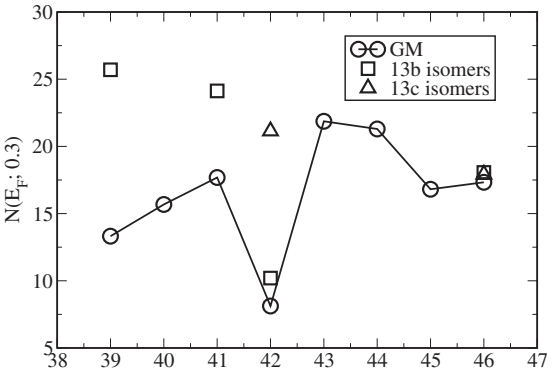

FIG. 5. Calculated values of $N(E_F;0.3)$ for GM and lowest energy isomers with $13b$ and $13c$ structures from Y to Pd (atomic numbers 39–46). The solid line connects the GMs of each element.

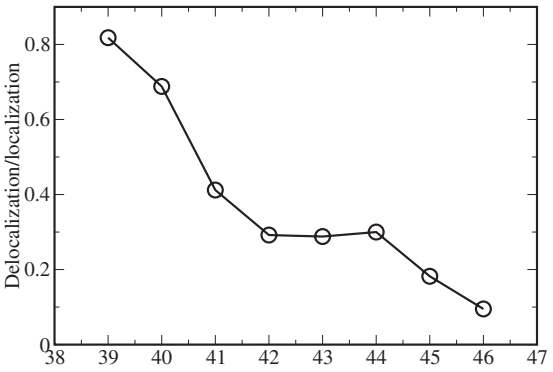

FIG. 6. Ratio of delocalized to localized electrons of the GM from Y to Pd (atomic numbers 39–46).

different structures ($13b$ and $13c$ structures in Fig. 1) are plotted along with those of GMs. Obviously, all the $13b$ and $13c$ isomers with higher energy also have higher $N(E_F;0.3)$ value, in line with the MHP again. Therefore, we suggest that metal clusters tend to obey a modified version of the MHP where the density of states near the Fermi level, not [(VIP)−(VEA)]/2 or the HOMO-LUMO gap, is the key variable. That is, metal clusters have a tendency to adopt geometric structures and spin states that minimize $N(E_F,w)$, where w is a suitable width [46].

D. Delocalization of valence electrons

Considering the geometric trend from ico to open cubic structure as the number of d electrons increase, it is worthwhile to analyze the character of valence electrons and the nature of bonding across the series of $4d$ metals. We performed natural population analysis calculations (with keyword NBO in the G03 software [47]) on all important cluster structures. The main results of these calculations are the number of *Lewis valence electrons* (i.e., effective number of localized electrons) and number of *non-Lewis valence electrons* (effective number of delocalized electrons). In Fig. 6, the ratio of delocalized to localized valence electrons from Y_{13} to Pd_{13} is plotted. The ratio decreases with increasing atomic number. This is because the effective screened nuclear charge felt by the outer-shell electrons increases from left to right in the $4d$ TM series and also because the ratio of the number of d-type to s-type electrons increases. So, in going from Y to Rh, orbitals become more localized and d-type bonding becomes more important. This correlates with the evolution of the structure from ico, to compact oblate, and finally cubic.

In order to describe the geometric trend, we use two descriptors. The first one is the mean atomic coordination c defined in the following way:

$$c = \frac{1}{13}\sum_j c_j,$$

$$c_j = \sum_{i \neq j} f(d_{ij}/d_0),$$

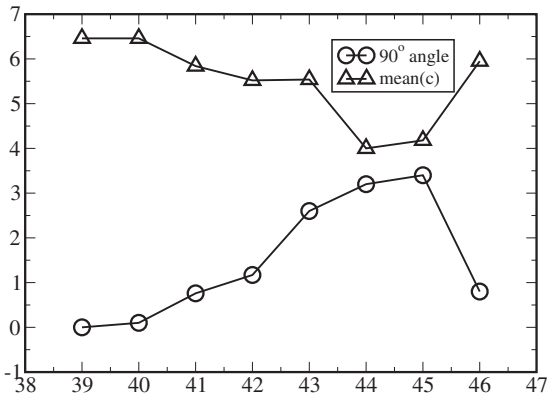

FIG. 7. Average number of 90° angles and mean coordination from Y to Pd (atomic numbers 39–46).

$$f(x) = 1 \quad \text{when} \quad x < 1.1$$
$$= (1.3 - x)/0.2 \quad \text{when} \quad 1.1 < x < 1.3$$
$$= 0 \quad \text{when} \quad 1.3 < x,$$

where d_0 is the average nearest-neighbor distance in the cluster. The second one is 1/13 of the number of 90° bond angles R defined as

$$R = \frac{1}{13} \sum_j \sum_{k_j > \ell_j} \cos(\theta_{k_j j \ell_j} - 90°)^{100},$$

where k_j and ℓ_j are indices for neighbors of atom j. The power 100 is arbitrary but produces R values that are intuitively meaningful. One might generally expect the mean atomic coordination c to be maximized in order to reduce surface energy, leading to ico GM. However, if d bonding is dominant one expects the number of 90° bonds R to be large in order to optimize the overlap between directional orbitals. Figure 7 shows an anticorrelation between c and R among the GM and variations across the $4d$ TM series that reflect the relative importance of s-type and d-type (directional) bondings. As the number of d electrons increases, there are more directional bonds which result in increasing R and decreasing c (directional bonds are more localized and require fewer nearest neighbors). Then R and c reach maximum and minimum values, respectively, at Rh_{13}. Pd_{13} shows similar c and R values as Y_{13} since the d orbitals in Pd are filled and the GM of Pd_{13} is an ico.

E. Thermochemical properties and ir spectra

Calculated thermochemical properties are useful to assess the possible coexistence of isomers in experiments. We calculated the zero-point energy (ZPE) correction, thermal enthalpies (H), and Gibbs free energies (G) of all the low-energy isomers. The results are in Tables III and IV. The Gibbs energy (G), or chemical potential, is minimized when a system reaches equilibrium at constant pressure and temperature, so it is probably the most relevant quantity in making comparisons to experiments and discussing the possible coexistence of isomers. Calculated relative G values (RG) on the order of 0.6 kcal/mol correspond to k_BT at room temperature (298 K) and suggest possible isomer coexistence. By this criterion, we find nearly equal RG values inside the following groups of isomers: $Y_{13a}(2S=13$ and $2S=17)$; $Nb_{13a}(2S=1)$ and $Nb_{13b}(2S=1)$; $Mo_{13a}(2S=0$ and $2S=2)$, $Mo_{13b}(2S=0)$, and $Mo_{13c}(2S=4)$; $Tc_{13}(2S=1$ and $2S=3)$; $Ru_{13}(2S=2,4,6)$; and $Rh_{13a}(2S=1$ and $2S=9)$. Generally, there are significant differences between the values of RE and RG. Small RG values suggest that nontrivial mixtures of structural isomers and/or spin states are quite likely. Note in particular Mo_{13} (three structural isomers and different spin states) and Rh_{13} (two very different spin states). The lowest vibrational frequencies we got for each cluster (they range from 15 to 84 cm^{-1}, see [19]) do not suggest liquidlike behavior, except maybe Zr_{13}. We do not put a lot of trust in the absolute values of cohesive energies we calculated for these clusters, but for completeness here they are for the GMs of Y_{13} to Pd_{13}, in that order, in eV/atom: 2.85, 4.65, 4.60, 3.55, 4.41, 4.05, 3.50, and 2.44.

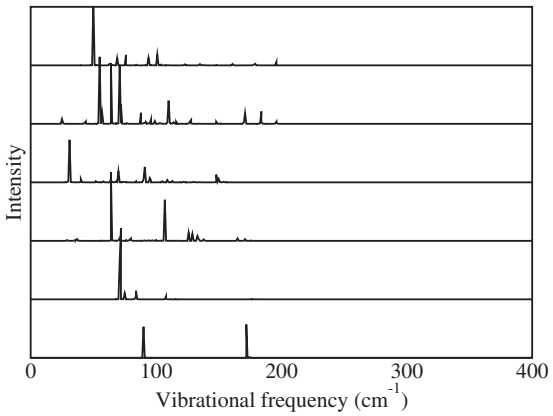

FIG. 8. Simulated ir spectra in the range 0–400 cm^{-1} for Y_{13} isomers with $2S=1$ (top), 7, 11, 13, 17, 19 (bottom).

Comparison between calculated and experimental vibrational spectra may allow deducing the atomic structures. Experiments were done by Fielicke and co-workers [49] for small vanadium and rhodium clusters. In Fig. 8 we show the distribution of intensity of all 33 vibrational frequencies for six Y_{13} isomers derived from the ico but with different $2S$ values. The features in the peaks distribution are very different from one isomer to another. It would be hard to distinguish individual clusters if the experimental spectra were generated by such mixtures of isomers. Even if there is only one structure, we may not be able to identify it from an ir spectrum. For example, the top two panels of Fig. 8 are not so different. Our findings are qualitatively similar for the cubic isomers of Rh_{13} (see [19]): small differences in magnetic moment (and structure) produce big differences in the simulated ir spectra. Figure 9 shows simulated ir spectra of GMs that are qualitatively different: $Y_{13a}(2S=19)$, $Nb_{13a}(2S=1)$, $Mo_{13a}(2S=0)$, $Tc_{13}(2S=0)$, and $Rh_{13a}(2S=1)$. Their ir spectra are obviously different from each other, as expected.

One possible experimental technique to distinguish different isomers is far-infrared resonance enhanced multiple photon dissociation (FIR-MPD) spectroscopy [50]. Using this technique, two Nb_9 isomers only 0.15 eV apart in energy

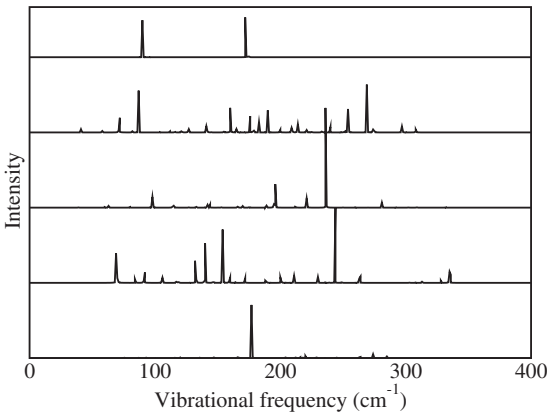

FIG. 9. Simulated ir spectra in the range 0–400 cm^{-1} for the GM of Y_{13} (top), Nb_{13}, Mo_{13}, Tc_{13}, and Rh_{13} (bottom).

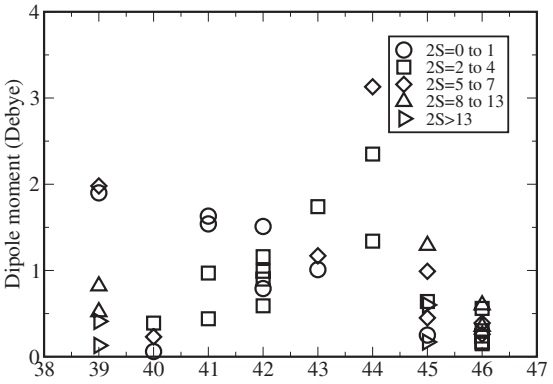

FIG. 10. Plot of dipole moment (Debye, D) for all isomers from Y to Pd (atomic numbers 39–46).

could be separated due to their different affinity to Ar atoms. If two isomers have sufficiently different electric-dipole moments, they will have different binding affinities to rare-gas atoms such as argon. The FIR-MPD spectra of their complex with rare-gas atoms will be different, reflecting their individual binding affinity. In Fig. 10 we plot the dipole moments for all the isomers listed in Tables III and IV. In some cases we see big differences in dipole moments. The following isomers might be separable by their different dipole moment values (in Debye, D): $Y_{13a}(2S=17)$ has a dipole moment μ of 0.13 D while $Y_{13a}(2S=13)$ has $\mu=0.52$ D; $Mo_{13a}(2S=0)$ has $\mu=0.79$ D while $Mo_{13b}(2S=0)$ has $\mu=1.51$ D; $Ru_{13}(2S=2)$ has $\mu=1.33$ D, $Ru_{13}(2S=4)$ has $\mu=2.35$ D, and $Ru_{13}(2S=6)$ has $\mu=3.13$ D; $Rh_{13a}(2S=0)$ has $\mu=0.25$ D, while $Rh_{13a}(2S=9)$ has $\mu=1.29$ D.

IV. CONCLUSION

We reported a systematic study of the structural, electronic, and magnetic properties of 13-atom 4*d* TM clusters from Y to Pd by using density-functional theory at the level of LSD, B3LYP, and PBE xc approximations. We considered not only the global minima [10] but also the lower energy isomers for different possible spin states and compared to available experimental and theoretical results. We found that orbitals formed by combination of *d* atomic orbitals become more localized in going from Y to Pd, and as a result the preferred cluster structures evolve from compact high-symmetry ico when the *d* bonds are delocalized (Y, Zr) to low symmetry and cubic when *d* bonds are localized (Ru, Rh), and finally ico again when there is essentially no *d* bonding (Pd). The calculated relative energies, ground-state magnetic moments, and the DOS near the Fermi level suggest a variant of the MHP: TM clusters have a *tendency* to adopt a geometry and electronic state that minimizes the DOS near the Fermi level. As a consequence, the spin magnetic moment is often relatively small in the lowest energy state. Our calculated $2S$ values generally agree with the available experimental results especially for Rh_{13}. The thermochemical properties suggest possible coexistence of isomers in the case of Y_{13}, Nb_{13}, Mo_{13}, Ru_{13}, and Rh_{13}. Coexistence of isomers would greatly complicate the analysis of experiments (infrared spectra, magnetic-moment measurements, etc.). Differences in calculated electric-dipole moments point to a possible way of separating isomers based on their different binding energies to rare-gas atoms [50].

ACKNOWLEDGMENTS

This work was made possible by the facilities of the Shared Hierarchical Academic Research Computing Network (SHARCNET) and support by the Natural Sciences and Engineering Research Council of Canada.

[1] F. Baletto and R. Ferrando, Rev. Mod. Phys. **77**, 371 (2005); S. Meng, E. G. Wang, and S. Gao, Phys. Rev. B **69**, 195404 (2004); S. Meng, L. F. Xu, E. G. Wang, and S. Gao, Phys. Rev. Lett. **89**, 176104 (2002).

[2] A. Fielicke, G. von Helden, G. Meijer, D. B. Pedersen, B. Simard, and D. M. Rayner, J. Phys. Chem. B **108**, 14591 (2004).

[3] H. Kietzmann, J. Morenzin, P. S. Bechthold, G. Gantefor, W. Eberhardt, D.-S. Yang, P. A. Hackett, R. Fournier, T. Pang, and C. Chen, Phys. Rev. Lett. **77**, 4528 (1996).

[4] M. B. Knickelbein and S. Yang, J. Chem. Phys. **93**, 5760 (1990).

[5] Y.-C. Bae, V. Kumar, H. Osanai, and Y. Kawazoe, Phys. Rev. B **72**, 125427 (2005).

[6] C. M. Chang and M. Y. Chou, Phys. Rev. Lett. **93**, 133401 (2004).

[7] L. L. Wang and D. D. Johnson, Phys. Rev. B **75**, 235405 (2007).

[8] S. Li, H. Li, J. Liu, X. Xue, Y. Tian, H. He, and Y. Jia, Phys. Rev. B **76**, 045410 (2007).

[9] J. Rogan, G. Garcia, C. Loyola, W. Orellana, R. Ramirez, and M. Kiwi, J. Chem. Phys. **125**, 214708 (2006).

[10] Y. Sun, M. Zhang, and R. Fournier, Phys. Rev. B **77**, 075435 (2008).
[11] M. Knickelbein, J. Chem. Phys. **102**, 1 (1995).
[12] H. Kietzmann, J. Morenzin, P. S. Bechtold, G. Gantefor, and W. Eberhardt, J. Chem. Phys. **109**, 2275 (1998).
[13] M. B. Knickelbein, Phys. Rev. B **71**, 184442 (2005).
[14] A. J. Cox, J. G. Louderback, S. E. Apsel, and L. A. Bloomfield, Phys. Rev. B **49**, 12295 (1994).
[15] H. K. Yuan, H. Chen, A. L. Kuang, A. S. Ahmed, and Z. H. Xiong, Phys. Rev. B **75**, 174412 (2007).
[16] J. Cheng and R. Fournier, Theor. Chem. Acc. **112**, 7 (2004).
[17] M. J. Frisch, G. W. Trucks, H. B. Schlegel, G. E. Scuseria, M. A. Robb, J. R. Cheeseman, J. A. Montgomery, Jr., T. Vreven, K. N. Kudin, J. C. Burant, J. M. Millam, S. S. Iyengar, J. Tomasi, V. Barone, B. Mennucci, M. Cossi, G. Scalmani, N. Rega, G. A. Petersson, N. Nakatsuji, M. Hada, M. Ehara, K. Toyota, R. Fukuda, J. Hasegawa, M. Ishida, T. Nakajima, Y. Honda, O. Kitao, H. Nakai, M. Klene, X. Li, J. E. Knox, H. P. Hratchian, J. B. Cross, V. Bakken, C. Adamo, J. Jaramillo, R. Gomperts, R. E. Stratmann, O. Yazyev, A. J. Austin, R. Cammi, C. Pomelli, J. W. Ochterski, P. Y. Ayala, K. Morokuma, G. A. Voth, P. Salvador, J. J. Dannenberg, V. G. Zakrzewski, S. Dapprich, A. D. Daniels, M. C. Strain, O. Farkas, D. K. Malick, A. D. Rabuck, K. Raghavachari, J. B. Foresman, J. V. Ortiz, Q. Cui, A. G. Baboul, S. Clifford, J. Cioslowski, B. B. Stefanov, G. Liu, A. Liashenko, P. Piskorz, I. Komaromi, R. L. Martin, D. J. Fox, T. Keith, M. A. Al-Laham, C. Y. Peng, A. Nanayakkara, M. Challacombe, P. M. W. Gill, B. Johnson, W. Chen, M. W. Wong, C. Gonzalez, and J. A. Pople, GAUSSIAN03, Revision C.02.
[18] J. P. Perdew, K. Burke, and M. Ernzerhof, Phys. Rev. Lett. **77**, 3865 (1996); **78**, 1396(E) (1997).
[19] See EPAPS Document No. E-PLRAAN-79-113903 for details of geometry optimization methods, the simulated ir spectra of Rh_{13} isomers, a summary of vibrational frequency data, and the Cartesian coordinates of clusters shown in Fig. 1. For more information on EPAPS, see http://www.aip.org/pubservs/epaps.html.
[20] S. P. Walch and C. W. Bauschlicher, in *Comparison of Ab Initio Quantum Chemistry with Experiment for Small Molecules*, edited by R. J. Bartlett (Reidel, Dordrecht, 1985).
[21] G. Verhaegen, S. Smoes, and J. Drowart, J. Chem. Phys. **40**, 239 (1964).
[22] C. A. Arrington, T. Blume, M. D. Morse, M. Doverstaal, and U. Sassenberg, J. Phys. Chem. **98**, 1398 (1994).
[23] C.-C. Wang, R.-N. Zhao, and J.-G. Han, J. Chem. Phys. **124**, 194301 (2006).
[24] A. M. James, P. Kowalczyk, R. Fournier, and B. Simard, J. Chem. Phys. **99**, 8504 (1993).
[25] D. A. Hales, L. Lian, and P. B. Armentrout, Int. J. Mass Spectrom. Ion Process. **102**, 269 (1990).
[26] S. K. Gupta, M. Pelino, and K. A. Gingerich, J. Phys. Chem. **83**, 2335 (1979).
[27] A. M. James, P. Kowalczyk, E. Langlois, M. D. Campbell, A. Ogawa, and B. Simard, J. Chem. Phys. **101**, 4485 (1994).
[28] M. D. Morse, Chem. Rev. (Washington, D.C.) **86**, 1049 (1986).
[29] J. B. Hopkins, P. R. R. Langridge-Smith, M. D. Morse, and R. E. Smalley, J. Chem. Phys. **78**, 1627 (1983).
[30] L. Brewer and J. S. Winn, Faraday Symp. Chem. Soc. **14**, 126 (1980).
[31] D. L. Cocke and K. A. Gingerich, J. Chem. Phys. **60**, 1958 (1974).
[32] L. Shim and K. A. Gingerich, J. Chem. Phys. **80**, 5107 (1984).
[33] S. Taylor, E. M. Spain, and M. D. Morse, J. Chem. Phys. **92**, 2710 (1990).
[34] V. Kumar and Y. Kawazoe, Phys. Rev. B **65**, 125403 (2002).
[35] W. Fa, C. Luo, and J. Dong, Phys. Rev. B **71**, 245415 (2005).
[36] D. Kaiming, Y. Jinlong, X. Chuanyun, and W. Kelin, Phys. Rev. B **54**, 11907 (1996).
[37] W. Zhang, X. Ran, H. Zhang, and L. Wang, J. Chem. Phys. **121**, 7717 (2004).
[38] T. Futschek, M. Marsman, and J. Hafner, J. Phys.: Condens. Matter **17**, 5927 (2005).
[39] B. I. Dunlap, Phys. Rev. A **41**, 5691 (1990).
[40] W. D. Knight, K. Clemenger, W. A. deHeer, W. A. Saunders, M. Y. Chou, and M. L. Cohen, Phys. Rev. Lett. **52**, 2141 (1984).
[41] F. Aguilera-Granja, J. L. Rodriguez-Lopez, K. Michaelian, E. O. Berlanga-Ramirez, and A. Vega, Phys. Rev. B **66**, 224410 (2002).
[42] E. P. Wohlfarth, J. Inst. Math. Appl. **4**, 359 (1968).
[43] R. G. Pearson, J. Chem. Educ. **45**, 981 (1968); R. G. Pearson, Acc. Chem. Res. **26**, 250 (1993).
[44] M. K. Harbola, Proc. Natl. Acad. Sci. U.S.A. **89**, 1036 (1992).
[45] R. G. Parr and P. K. Chattaraj, J. Am. Chem. Soc. **113**, 1854 (1991); P. W. Ayers and R. G. Parr, *ibid.* **122**, 2010 (2000).
[46] The width w should be large enough to define an energy window that contains at least a few energy levels and should at the same time be a small fraction of the band width. With these criteria w is not defined precisely, but it is on the order of 0.3 eV for 13-atom 4*d* TM clusters.
[47] A. E. Reed, L. A. Curtiss, and F. Weinhold, Chem. Rev. (Washington, D.C.) **88**, 899 (1988).
[48] J. W. Ochterski, http://www.gaussian.com
[49] C. Ratsch, A. Fielicke, A. Kiriyuk, J. Behler, G. von Helden, G. Meijer, and M. Scheffler, J. Chem. Phys. **122**, 124302 (2005); A. Fielicke, G. von Helden, G. Meijer, D. B. Pedersen, B. Simard, and D. M. Rayner, J. Phys. Chem. B **108**, 14591 (2004).
[50] A. Fielicke, C. Ratsch, G. von Helden, and G. Meijer, J. Chem. Phys. **122**, 091105 (2005).